5-24-2010

Doped-Ceria Diffusion Barriers Prepared by Infiltration for Solid Oxide Fuel Cells

Rainer Küngas
University of Pennsylvania, kungas@seas.upenn.edu

Fred Bidrawn
University of Pennsylvania, fbidrawn@seas.upenn.edu

John M. Vohs
University of Pennsylvania, vohs@seas.upenn.edu

Raymond J. Gorte
University of Pennsylvania, gorte@seas.upenn.edu

Suggested Citation:
Küngas, R., Bidrawn, F. Vohs, J.M. and Gorte, R.J. (2010). "Doped-Ceria Diffusion Barriers Prepared by Infiltration for Solid Oxide Fuel Cells." *Electrochemical and Solid-State Letters.* 13 (8) B87-B90.

Publisher URL: http://dx.doi.org/10.1149/1.3432253

Doped-Ceria Diffusion Barriers Prepared by Infiltration for Solid Oxide Fuel Cells

Abstract
To stabilize solid oxide fuel cells cathodes prepared by infiltration of $La_{0.8}Sr_{0.2}CoO_3$ (LSCo) into porous yttria-stabilized zirconia (YSZ), a coating of Sm-doped ceria (SDC) was first deposited onto the YSZ scaffold. The dense SDC coating was prepared by infiltration with aqueous solutions of $SM(NO_3)_3$ and $Ce(NO_3)_3$, followed by calcination to 1473 K. The SDC coating prevented ~ 20 mΩ cm^2, at 973 K, with acceptable degradation after heating to 1373 K.

Disciplines
Biochemical and Biomolecular Engineering | Chemical Engineering | Engineering

Comments
Suggested Citation:
Küngas, R., Bidrawn, F. Vohs, J.M. and Gorte, R.J. (2010). "Doped-Ceria Diffusion Barriers Prepared by Infiltration for Solid Oxide Fuel Cells." *Electrochemical and Solid-State Letters.* 13 (8) B87-B90.

Publisher URL: http://dx.doi.org/10.1149/1.3432253

Electrochemical and Solid-State Letters, **13** (8) B87-B90 (2010)
1099-0062/2010/13(8)/B87/4/$28.00 © The Electrochemical Society

Doped-Ceria Diffusion Barriers Prepared by Infiltration for Solid Oxide Fuel Cells

R. Küngas,* F. Bidrawn, J. M. Vohs, and R. J. Gorte**,z**

Department of Chemical and Biomolecular Engineering, University of Pennsylvania, Philadelphia, Pennsylvania 19104, USA

To stabilize solid oxide fuel cell cathodes prepared by infiltration of $La_{0.8}Sr_{0.2}CoO_3$ (LSCo) into porous yttria-stabilized zirconia (YSZ), a coating of Sm-doped ceria (SDC) was first deposited onto the YSZ scaffold. The dense SDC coating was prepared by infiltration with aqueous solutions of $Sm(NO_3)_3$ and $Ce(NO_3)_3$, followed by calcination to 1473 K. The SDC coating prevented solid-state reactions between LSCo and YSZ at 1373 K. LSCo–SDC/YSZ electrodes exhibited low cathode impedances, ~ 20 mΩ cm^2, at 973 K, with acceptable degradation after heating to 1373 K.
 [DOI: 10.1149/1.3432253]

Manuscript submitted April 1, 2010; revised manuscript received April 27, 2010. Published May 24, 2010. This was Paper 1386 presented at the Vienna, Austria, Meeting of the Society, October 4–9, 2009.

The most commonly used material for cathodes in solid oxide fuel cells is a composite of Sr-doped $LaMnO_3$ (LSM) and yttria-stabilized zirconia (YSZ), with the LSM in the composite providing electronic conductivity and catalytic activity for oxygen reduction. The addition of YSZ to the electrode provides ionic conductivity to increase the length of the three-phase boundary by providing ion-conducting channels from the electrolyte into the electrode.[1] In most cases, LSM–YSZ composites are prepared by sintering a mixture of LSM and YSZ powders onto the YSZ electrolyte. Relatively high temperatures ($> \sim 1300$ K)[2] are required to sinter the YSZ particles in the electrode to the electrolyte. Significantly improved performance can be achieved by replacing LSM with mixed conducting perovskites, such as Sr-doped $LaCoO_3$ (LSCo),[3-7] $LaFeO_3$ (LSF),[8-12] or $LaCo_xFe_{(1-x)}O_3$ (LSCF);[13,14] however, it is not possible to cofire these perovskites with YSZ at the temperatures required for sintering the YSZ phase because this leads to either reaction with the YSZ or other effects that lower the electrode performance.[15,16]

Recently, composite electrodes have been prepared without high temperature sintering of the perovskite phase using infiltration.[16-18] In this case, a porous YSZ scaffold is first sintered together with the electrolyte, and the perovskite is then added in subsequent steps by infiltrating the porous YSZ with solutions that contain either the nanoparticles of the perovskites or the appropriate cations for synthesizing the perovskites in situ.[19,20] Composites prepared by infiltration have two main advantages over composites prepared by traditional approaches. First, the sintering temperature for the YSZ component of the composite can be much higher than the sintering temperature used for the perovskite. Because the YSZ scaffold can be sintered to the electrolyte at very high temperatures, the ion-conducting channels from the electrolyte into the electrode are well established and delamination of electrodes is typically not a problem. Second, because the conducting phase is added to an existing YSZ scaffold, the composites formed by infiltration are not random. One implication of the nonrandom structure is that sufficient conductivity can be achieved using perovskite loadings below the normal percolation threshold of 30 vol %.[16,21] Another consequence of the nonrandom structure is that the coefficients of thermal expansion (CTE) of the composite are closer to that of YSZ scaffold than to the weighted average of the components.[6]

Composites of LSCo and YSZ have provided very low cathode impedances when prepared by infiltration;[6,22] however, the impedance has increased dramatically with time or increased calcination temperature. Degradation with LSCo is likely due to solid-state reactions, which have occurred between YSZ and $LaCoO_3$ at temperatures as low as 973 K.[23] The usual approach to preventing solid-state reactions between perovskites and YSZ involves incorporating a thin layer of doped ceria [e.g., $Ce_{0.8}Sm_{0.2}O_{1.9}$ (SDC)] between the electrolyte and the electrode in a manner similar to what is shown in Fig. 1a.[24,25] This approach is successfully applied with cathodes based on LSCF.[26] However, the incorporation of barrier layers does not prevent problems of CTE mismatch or mechanical instability. Furthermore, a recent comparison of LSM cathodes with and without doped-ceria layers indicated that doped ceria layer may alter performance in a more complicated manner.[27]

In the present study, we set out to test an alternative method for incorporating a barrier layer, shown schematically in Fig. 1b. The concept was to coat the porous YSZ scaffold with SDC before infiltration with the conducting perovskite. Electrodes prepared in this manner exhibit the advantages associated with infiltrated electrodes (e.g., less LSCo required for conductivity, better CTE match, and better stability toward delamination) while minimizing problems associated with solid-state reactions at the LSCo–YSZ interface.

Experimental

The electrode performances in this study were measured using symmetric cells. The first step in cell fabrication involved making a porous–dense–porous YSZ wafer using tape-casting methods, as described in detail elsewhere.[28] After sintering the tapes at 1773 K for 4 h, the dense electrolyte layers were 88 ± 5 μm thick and 1 cm in diameter, while the two porous layers were each 55 ± 2 μm thick and 0.67 cm in diameter. Based on an earlier work, the porous layers were between 60 and 65% porous.[28] To prepare an SDC barrier coating, an aqueous mixture of $Ce(NO_3)_3 \cdot 6H_2O$ (Alfa Aesar, 99.5%) and $Sm(NO_3)_3 \cdot 6H_2O$ (Alfa Aesar, 99.9%) was infiltrated into the porous YSZ layers, followed by heating in air to 723 K. Infiltration steps were repeated until the desired loading had been achieved. The cells were then fired to temperatures up to 1473 K for 4 h.

The LSCo–YSZ and LSCo–SDC–YSZ electrodes were prepared by infiltration of the porous YSZ or the SDC–YSZ scaffolds with an aqueous solution consisting of $La(NO_3)_3 \cdot 6H_2O$ (Alfa Aesar, 99.9%), $Sr(NO_3)_2$ (Alfa Aesar, 99%), and $Co(NO_3) \cdot 6H_2O$ (Aldrich, 99%) at a molar ratio of La:Sr:Co = 0.8:0.2:1. Citric acid, in a 1:1 ratio with the metal cations, was used as a complexing agent to form the perovskite at lower temperatures. The use of a complexing agent is critical because new phases, indicative of a solid-state reaction with the YSZ, were formed at much lower temperatures when citric acid was not included. Furthermore, the reproducibility of the electrochemical test results improves significantly when a complexing agent was used. Each infiltration was followed by heat-treatment in air at 723 K. Multiple infiltration steps were needed to reach the final loading of 35 wt % (~ 20 vol %). To form the desired perovskite structure, the cells were heated in air to 973 K for 4 h before applying Ag paste for current collection. The cells were then attached to an alumina rod using a ceramic adhesive (Aremco, Ceramabond 552). Electrochemical impedance spectra were recorded us-

* Electrochemical Society Student Member.
** Electrochemical Society Active Member.
z E-mail: gorte@seas.upenn.edu

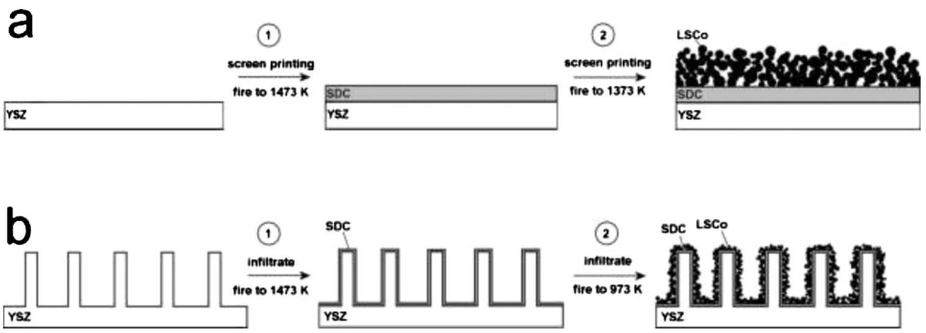

Figure 1. Schematic comparison of (a) traditional and (b) proposed approach to preparing SDC diffusion barrier layers.

ing a Gamry Instruments potentiostat in the frequency range of 0.1 Hz to 100 kHz and with an ac perturbation of 5 mA, with the samples held in ambient air. All of the impedances in this paper have been divided by 2 to account for there being two electrodes.

Brunauer, Emmett, and Teller (BET) and X-ray diffraction (XRD) characterizations were carried out on $3 \times 3 \times 10$ mm slabs, prepared from the same slurries that were used in the tape-casting process for the porous YSZ. XRD patterns were measured using Cu Kα radiation. BET isotherms were measured using Kr adsorption at 78 K and were used to determine surface areas. Scanning electron microscopy (SEM) coupled with an energy-dispersive X-ray analyzer (FEI Quanta 600 FESEM) was used to determine the microstructure and elemental distribution of prepared cells.

Results and Discussion

In earlier studies of ceria incorporation into YSZ scaffolds, ceria formed a porous coating of nanoparticles over the porous YSZ following calcination at temperatures below 1123 K, with increasingly dense films being formed at calcination temperatures above 1473 K.[29] Because the doped-ceria interlayers must be dense to effectively prevent interfacial reactions,[26] we first investigated the effect of sintering temperature on the morphology of SDC in YSZ using SEM and BET isotherms.

The SEM results for the SDC coatings are shown in Fig. 2. Figure 2a is a micrograph of the empty YSZ scaffold. The pore structure has an appearance similar to that of a sponge, with pores ranging between 0.5 and 3 μm. After adding 20 wt % (~10 vol %) SDC with calcination to 1373 K, the YSZ scaffold is covered by well-defined particles that are much less than 0.1 μm in diameter. There appear to be gaps between the particles that would allow fluid-phase species to interact with the underlying YSZ. The SDC particles grow dramatically after heating to 1473 K (Fig. 2c), forming crystallites that are 0.2–0.3 μm and that completely cover the YSZ scaffold. An energy dispersive X-ray analysis (EDX) scan along the line A–B in Fig. 2c and d demonstrated that Ce was evenly distributed on the surface of the underlying YSZ. The peaks in the Ce concentration in this line scan correspond to the edges of the original YSZ features, where the SDC film appears thicker to the electron beam used in the EDX measurement. There were no signs of phase segregation or of large blocks of SDC anywhere in the sample.

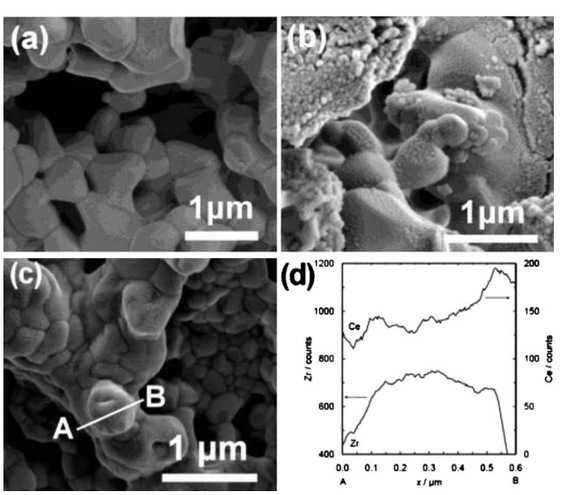

Figure 2. The microstructure of (a) the YSZ matrix and YSZ–SDC composites with 20 wt % SDC fired to (b) 1373 and (c) 1473 K. The result of an EDX scan along the path A–B is shown in (d).

Data from the BET isotherms, shown in Table I, confirm the above picture. In the absence of added SDC, the YSZ scaffold had a surface area of 0.27 m^2/g. For a material with uniform cylindrical pores, a porosity of 65%, and walls having the bulk density of YSZ, the average pore diameter is calculated to be ~3 μm,[30] a value that agrees reasonably with the SEM measurements. Following the addition of 20 wt % SDC and calcination to 1123 K, the surface area increased to 1.2 m^2/g due to the presence of small SDC particles. Only after calcination to 1473 K did the specific surface area of the SDC–YSZ composite decrease below that of the original YSZ, indicating the formation of a dense film of SDC over the YSZ. Further heating to 1573 K had a minimal effect on the surface area.

Because SDC can react with YSZ to form solid solutions,[31] XRD measurements of 40 wt % (~20 vol %) SDC in YSZ were performed as a function of temperature, as shown in Fig. 3. There were no changes in the YSZ peaks at 30.17 and 35.12° as the temperature was increased from 973 to 1473 K, and features associated with SDC at 28.43 and 32.95° simply narrowed due to increasing crystallite size. At 1523 K, there was a shifting of both the SDC and the YSZ peaks because of the formation of solid solutions at the interface. At 1573 K, the extent of the solid-state reaction between SDC and YSZ is such that the XRD pattern is nearly that of a single-phase oxide.

Figure 4 summarizes the XRD results obtained following the addition of 20 vol % LSCo into the YSZ scaffold with varying heat-treatments. The patterns in Fig. 4a through e were obtained without an SDC coating, while that in Fig. 4f corresponds to a

Table I. BET surface areas of an empty YSZ scaffold and 20 wt % SDC in YSZ composite, shown as a function of SDC calcination temperature. The measurements were conducted on $3 \times 3 \times 10$ mm SDC/YSZ slabs.

		S_{BET} (m^2 g^{-1})
YSZ		0.27
SDC–YSZ calcined to	1123 K	1.24
	1273 K	0.57
	1373 K	0.39
	1473 K	0.24
	1573 K	0.21

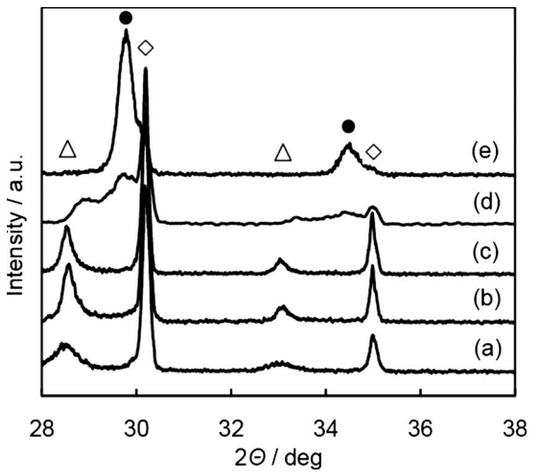

Figure 3. XRD patterns of the SDC/YSZ composite calcined to (a) 973, (b) 1373, (c) 1473, (d) 1523, and (e) 1573 K: (◇) YSZ, (△) SDC, and (●) $Ce_2Zr_3O_{10}$. The measurements were carried out on 3 × 3 × 10 mm SDC/YSZ slabs.

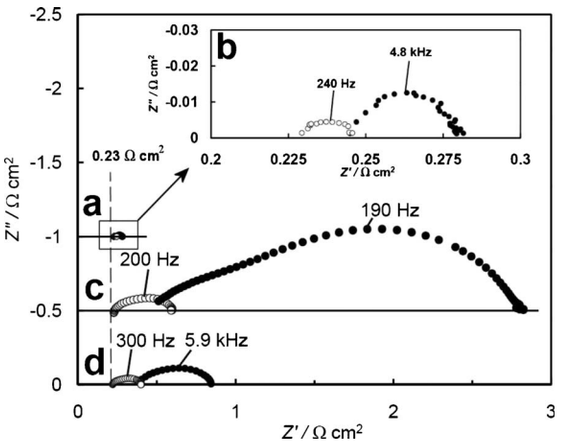

Figure 5. Electrochemical impedance spectra of LSCo–YSZ (filled symbols) and LSCo–SDC–YSZ (open symbols) symmetric cells at 973 K and ambient air conditions. LSCo calcination temperature was 973 K for (a) and (b) and 1373 K for (c) and (d). All measurements were carried out at open-circuit conditions, except for (d), where a current of 600 mA/cm^2 was applied.

sample in which 20 vol % SDC, calcined at 1473 K, was incorporated into the YSZ scaffold before adding LSCo. The pattern in Fig. 4b, contains a broad peak at 33° 2θ, demonstrating the formation of the perovskite phase after heating to only 973 K. The two underlying peaks, associated with the rhombohedral structure of the LSCo perovskite, are resolved after heating to 1123 K for 4 h due to improved crystallinity (Fig. 4c). By 1273 K, the appearance of $La_2Zr_2O_7$ is evident from the peak at 28.59° 2θ. After calcining at 1373 K, the peak corresponding to $La_2Zr_2O_7$ has grown larger, and an additional feature at 30.86° 2θ due to $SrZrO_3$ is observed.

In a previous study of the stability of cathodes formed by infiltration of LSF into porous YSZ, calcination to 1373 K caused similar changes to the cathode as those observed after fuel cell operation at 973 K for several thousands of hours.[15] Assuming that a similar correlation exists between operating time and calcination temperature for the LSCo–YSZ composites, the observation of new phases in the XRD data in Fig. 4d and e implies that LSCo–YSZ electrodes are not stable. Therefore, to prevent a solid-state reaction between LSCo and YSZ, we first incorporated 20 vol % SDC into the YSZ, followed by calcination to 1473 K, before again adding 20 vol % LSCo. The diffraction pattern in Fig. 4f was obtained from this composite after calcination to 1373 K for 4 h. While overlap of features associated with SDC and $La_2Zr_2O_7$ near 28.5° 2θ prevents us from seeing whether $La_2Zr_2O_7$ is formed, there is no evidence in the XRD pattern for features corresponding to $SrZrO_3$, suggesting that the SDC layer has prevented the solid-state reactions. Slight broadening of the YSZ peaks at 30.17 and 35.12° 2θ can be detected in pattern (f) in Fig. 4. This effect is likely to be caused by the onset of a solid-state reaction between YSZ and SDC. However, we found samples with SDC layers calcined to either 1373 or 1573 K to be much less effective in stabilizing the LSCo. SDC layers calcined to 1373 K are not dense enough to provide an effective barrier, while layers fired to 1573 K showed an extensive reaction between YSZ and SDC.

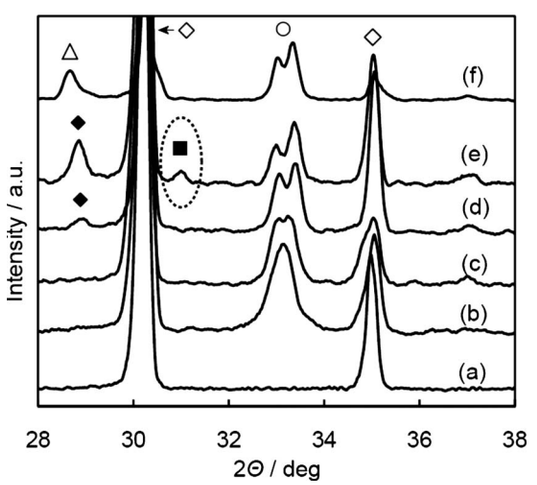

Figure 4. XRD patterns of (a) blank YSZ, [(b)-(e)] LSCo-YSZ, and (f) LSCo–SDC/YSZ composites. Calcination temperatures: (b) 973, (c) 1123, (d) 1273, (e), and (f) both 1373 K. (◇) YSZ, (△) SDC, (○) LSCo, (♦) $La_2Zr_2O_7$, and (■) $SrZrO_3$.

Electrode performance and stability are the most important tests of the effectiveness of the SDC layer. To determine the effect of the SDC layer, impedance data were measured at 973 K using symmetric cells having 20 vol % LSCo, with and without 20 vol % SDC, following calcination at 973 and 1373 K. The impedance data, reported as Cole–Cole plots in Fig. 5, have all been divided by 2 to account for the presence of two electrodes. After calcination to 973 K, the performances of both composite electrodes were very good (Fig. 5a and b). The resistance of an 88 μm YSZ electrolyte at 973 K is calculated to be 0.46 Ω cm^2,[32] so that the high frequency intercepts at 0.23 and 0.25 Ω cm^2 for the cells with and without SDC are close to 50% of the expected resistance of the electrolyte. The nonohmic losses, ~20 and 30 mΩ cm^2 for cells with and without SDC, respectively, are also both very good.

The effect of the SDC layer is clearly seen in the impedances measured on cells that had been calcined to 1373 K (Fig. 5c). Without SDC, ohmic losses have increased to 0.5 Ω cm^2 and the nonohmic losses have increased to 2.3 Ω cm^2. However, with the SDC layer, the ohmic losses remain unchanged and the nonohmic losses have increased to a more acceptable value of ~0.3 Ω cm^2. The reason for the increased impedance in the absence of SDC is almost certainly associated with solid-state reactions that form insulating phases at the LSCo–YSZ interface. With the SDC, we suggest that the increase in impedance is due to the coarsening of the perovskite particles, as seen in Fig. 6, and a subsequent loss in the three-phase boundary sites. Previous work on the infiltration of less reactive perovskites also saw increased impedances following higher calcination temperatures that appeared to be due to particle coarsening.[33,34] Studies by Jørgensen et al. on LSM/YSZ composite electrodes also support this conclusion.[35]

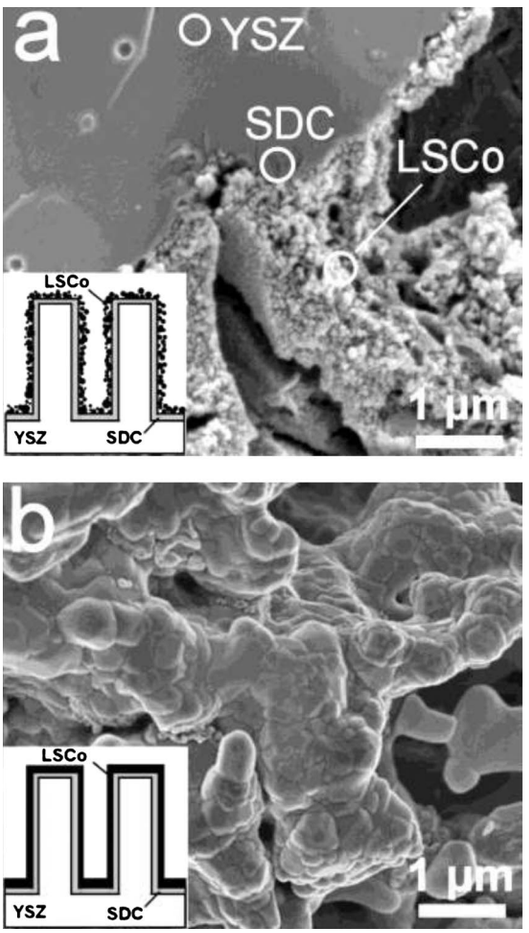

Figure 6. SEM images of an LSCo–SDC–YSZ electrode calcined to (a) 973 and (b) 1373 K. The composition of points marked with open circles in (a) were determined by EDX.

The impedances for the cells that had been calcined to 1373 K overestimate the losses that would be observed during fuel cell operation. As shown in Fig. 5d, when a current of 600 mA/cm^2 was applied to the symmetric cells, the nonohmic losses decreased to 0.15 Ω cm^2 for the cell with SDC and 0.43 Ω cm^2 for cell without. Although application of a current makes the cells asymmetric, with one electrode operating anodically and the other cathodically, the cathodic impedances of the cells cannot be larger than the sum of the impedances of the two electrodes. Therefore, the electrode impedances for the two cells decrease with current density. This was also observed with LSF–YSZ electrodes calcined to higher temperatures and, again, appears to be due to the coarsening of the perovskite nanoparticles.[33,34]

Although the impedances of the electrode prepared by infiltration of LSCo into a YSZ scaffold with an SDC barrier in this study was good, this can almost certainly be improved. For example, a previous work showed that the pore structure of the YSZ scaffold can have a large impact on electrode impedance.[6] We made no attempt to optimize this pore structure in the present investigation. We also did not investigate whether there is an optimal thickness for the SDC layer.

The additional steps required for fabricating electrodes by infiltration are a barrier to adopting this procedure, particularly when an SDC film must first be added into the YSZ scaffold to prevent solid-state reactions between the YSZ and the perovskite. However, the present results show that one can use this method to make high performance electrodes, with good stability, from materials that are not well matched for CTE. The fact that the YSZ scaffold is heated together with the electrolyte to very high temperatures also ensures that these electrodes adhere well to the electrolyte. Therefore, this approach is worth considering as a method for producing high performance cathodes.

Conclusion

The possibility of preparing a samaria-doped ceria diffusion barrier layer by infiltration methods was investigated. The best results were observed when the SDC was calcined to 1473 K. Both electrode impedances measured on symmetric cells and XRD data suggest that such layers are effective in reducing the extent of the solid-state reaction between LSCo and YSZ.

Acknowledgment

This work was funded by the U.S. Department of Energy's Hydrogen Fuel Initiative (grant DE-FG02-05ER15721).

University of Pennsylvania assisted in meeting the publication costs of this article.

References

1. C. W. Tanner, K.-Z. Fung, and A. V. Virkar, *J. Electrochem. Soc.*, **144**, 21 (1997).
2. J. Mertens, V. A. C. Haanappel, C. Wedershoven, and H.-P. Buchkremer, *J. Fuel Cell Sci. Technol.*, **3**, 415 (2006).
3. H. Uchida, S. Arisaka, and M. Watanabe, *Solid State Ionics*, **135**, 347 (2000).
4. T. Horita, K. Yamaji, N. Sakai, H. Yokokawa, A. Weber, and E. Ivers-Tiffee, *Electrochim. Acta*, **46**, 1837 (2001).
5. S. J. Skinner, *Int. J. Inorg. Mater.*, **3**, 113 (2001).
6. Y. Huang, K. Ahn, J. M. Vohs, and R. J. Gorte, *J. Electrochem. Soc.*, **151**, A1592 (2004).
7. R. Küngas, I. Kivi, K. Lust, G. Nurk, and E. Lust, *J. Electroanal. Chem.*, **629**, 94 (2009).
8. J. M. Ralph, C. Rossignol, and R. Kumar, *J. Electrochem. Soc.*, **150**, A1518 (2003).
9. S. P. Simner, J. F. Bonnett, N. L. Canfield, K. D. Meinhardt, V. L. Sprenkle, and J. W. Stevenson, *Electrochem. Solid-State Lett.*, **5**, A173 (2002).
10. S. P. Simner, J. F. Bonnett, N. L. Canfield, K. D. Meinhardt, J. P. Shelton, V. L. Sprenkle, and J. W. Stevenson, *J. Power Sources*, **113**, 1 (2003).
11. S. P. Simner, M. D. Anderson, and J. W. Stevenson, *J. Am. Ceram. Soc.*, **87**, 1471 (2004).
12. Y. Huang, J. M. Vohs, and R. J. Gorte, *J. Electrochem. Soc.*, **151**, A646 (2004).
13. S. P. Jiang, *Solid State Ionics*, **146**, 1 (2002).
14. A. Esquirol, N. P. Brandon, J. A. Kilner, and M. Mogensen, *J. Electrochem. Soc.*, **151**, A1847 (2004).
15. W. Wang, M. D. Gross, J. M. Vohs, and R. J. Gorte, *J. Electrochem. Soc.*, **154**, B439 (2007).
16. J. M. Vohs and R. J. Gorte, *Adv. Mater.*, **21**, 943 (2009).
17. M. D. Gross, J. M. Vohs, and R. J. Gorte, *J. Mater. Chem.*, **17**, 3071 (2007).
18. R. Craciun, S. Park, R. J. Gorte, J. M. Vohs, C. Wang, and W. L. Worrell, *J. Electrochem. Soc.*, **146**, 4019 (1999).
19. S. P. Jiang, *Mater. Sci. Eng., A*, **418**, 199 (2006).
20. Y. Huang, J. M. Vohs, and R. J. Gorte, *Electrochem. Solid-State Lett.*, **9**, A237 (2006).
21. H. P. He, Y. Huang, J. Regal, M. Boaro, J. M. Vohs, and R. J. Gorte, *J. Am. Ceram. Soc.*, **87**, 331 (2004).
22. T. J. Armstrong and J. G. Rich, *J. Electrochem. Soc.*, **153**, A515 (2006).
23. M. Sase, D. Ueno, K. Yashiro, A. Kaimai, T. Kawada, and J. Mizusaki, *J. Phys. Chem. Solids*, **66**, 343 (2005).
24. M. Shiono, K. Kobayashi, T. L. Nguyen, K. Hosoda, T. Kato, K. Ota, and M. Dokiya, *Solid State Ionics*, **170**, 1 (2004).
25. C. Rossignol, J. M. Ralph, J.-M. Bae, and J. T. Vaughey, *Solid State Ionics*, **175**, 59 (2004).
26. S. Uhlenbruck, T. Moskalewicz, N. Jordan, H.-J. Penkalla, and H. P. Buchkremer, *Solid State Ionics*, **180**, 418 (2009).
27. K. Kammer Hansen, M. Menon, J. Knudsen, N. Bonanos, and M. Mogensen, *J. Electrochem. Soc.*, **157**, B309 (2010).
28. S. Park, R. J. Gorte, and J. M. Vohs, *J. Electrochem. Soc.*, **148**, A443 (2001).
29. G. Kim, J. M. Vohs, and R. J. Gorte, *J. Mater. Chem.*, **18**, 2386 (2008).
30. Y. Huang, J. M. Vohs, and R. J. Gorte, *J. Electrochem. Soc.*, **152**, A1347 (2005).
31. G. Kim, M. D. Gross, W. Wang, J. M. Vohs, and R. J. Gorte, *J. Electrochem. Soc.*, **155**, B360 (2008).
32. K. Sasaki and J. Maier, *Solid State Ionics*, **134**, 303 (2000).
33. S. Lee, M. Bevilacqua, P. Fornasiero, J. M. Vohs, and R. J. Gorte, *J. Power Sources*, **193**, 747 (2009).
34. F. Bidrawn, G. Kim, N. Aramrueang, J. M. Vohs, and R. J. Gorte, *J. Power Sources*, **195**, 720 (2010).
35. M. J. Jørgensen, S. Primdahl, C. Bagger, and M. Mogensen, *Solid State Ionics*, **139**, 1 (2001).